grants to R.T.O. and N.P.C.W. and a postdoctoral fellowship to R.T.B.

Registry No. 1 (R = H), 118436-74-1; 1 (R = CF_3), 118436-72-9; 1 (R = Cl), 118436-69-4; 1 (R = Ph), 118436-79-6; 1 (R = 4-$MeOC_6H_4$), 118436-80-9; 1 (R = 4-$NO_2C_6H_4$), 118436-78-5; 2 (R = H), 118436-73-0; 2 (R = CF_3), 118436-71-8; 2 (R = Cl), 118436-67-2; 2 (R = F), 118436-68-3; 2 (R = Br), 118436-66-1; 2 (R = Ph), 118436-77-4; 2 (R = CCl_3), 118436-70-7; 2 (R = Bu-t), 118436-76-3; 2 (R = Me), 118436-75-2; 3 (R = Ph), 94426-38-7; 3 (R = 4-$MeOC_6H_4$), 118377-76-7; 3 (R = $NO_2C_6H_4$), 118377-77-8; 3 (R = Cl), 58589-34-7; 3 (R = CF_3), 118377-78-9; 4 (R = F), 99344-85-1; 4 (R = Cl), 85175-36-6; 4 (R = Br), 99344-91-9; 4 (R = Ph), 63481-05-0; 4 (R = CF_3), 93842-58-1; 4 (R = CCl_3), 62635-18-1; 4 (R = Bu-t), 63432-63-3; 4 (R = Me), 82290-16-2; $S_3N_3Cl_3$, 5964-00-1; $CFCl_3$, 75-69-4; 4-methoxybenzamidine, 22265-37-8; 4-nitrobenzamidine, 25412-75-3; N-(perfluoroacetimidoyl)perfluoroacetamidine, 675-05-8; sulfur dichloride, 10545-99-0.

Polymerization and Decomposition of Acetaldehyde on Ru(001)

M. A. Henderson, Y. Zhou, and J. M. White*

Contribution from the Department of Chemistry, University of Texas, Austin, Texas 78712.
Received July 8, 1988

Abstract: The polymerization and decomposition of acetaldehyde (CH_3CHO) on Ru(001) was studied by high-resolution electron energy loss spectroscopy (HREELS), static secondary ion mass spectrometry (SSIMS), and temperature-programmed desorption (TPD). Evidence is presented that low exposures (<0.4 langmuir) of CH_3CHO on Ru(001) at 110 K polymerize across the surface in two dimensions upon adsorption. η^1(O) CH_3CHO, which is the proposed intermediate in surface polymerization, is stable only at exposures approaching saturation of the first layer (0.4–0.6 langmuir). This species incorporates into the surface polymer after heating above 150 K. Exposures above 0.6 langmuir result in multilayer CH_3CHO, which desorbs in TPD at 148 K. A second CH_3CHO state appears in TPD at 250 K for CH_3CHO exposures above 2 langmuir and is attributed to decomposition of polymerized CH_3CHO in three dimensions above the surface. Ions from this polymer, containing at least monomer units, are detected in +SSIMS. The surface polymer decomposes to η^2(C,O) CH_3CHO after heating above 250 K. Decomposition of the latter species at 315 K evolves H_2 in TPD and leaves CO and small amounts of C_xH and η^2(C,O) CH_3CO on the surface.

1. Introduction

Chemisorbed aldehydes have been proposed as key intermediates in the decomposition of primary alcohols on metal surfaces[1,2] and in secondary reactions of Fischer–Tropsch synthesis leading to oxygenates.[1] The structure of these intermediates is typically an η^2(C,O) bound species. McCabe et al.[3] proposed this structure as a minority species from acetaldehyde (CH_3CHO) on Pt(S)-[6(11)×(100)], and Anton et al. have observed it for formaldehyde (H_2CO) Ru(001).[4] Recently, we have observed η^2(C,O) CH_3CHO from the hydrogenation of ketene (CH_2CO) on Ru(001).[5-7]

In a continuing effort to understand the chemistry of small oxygen-containing molecules on metal surfaces, we have studied the interaction of acetaldehyde with Ru(001) by high-resolution electron energy loss spectroscopy (HREELS), positive static secondary ion mass spectrometry (+SSIMS), and temperature-programmed desorption (TPD). We find that CH_3CHO adsorption on Ru(001) at 110 K is very complex, exhibiting at least four different states, attributed to η^1(O), two polymerized forms, and multilayer. Decomposition of one of the polymer species at 250 K results in η^2(C,O) CH_3CHO. This species is not observed upon adsorption at 110 K, but it is responsible for all the H_2, CO, and trace CO_2 observed in TPD. Polymerization of CH_3CHO has been observed in hydrocarbon solutions,[8-14] on oxides,[15] and in matrix media[16] but not without the influence of an inorganic acid or organometallic initiator. In UHV experiments, Madix et al.[17] were the first to observe CH_3CHO polymerization, as the cyclic trimer paraldehyde, from CH_3CHO adsorbed on a p(2×2) S-covered Ni(100) surface.

2. Experimental Section

The ultrahigh-vacuum chamber used in this study and the methods of data collection have been detailed elsewhere.[18] The system is ion-pumped with a working base pressure of 1×10^{-10} Torr. The HREELS

(1) Benziger, J. B.; Madix, R. J. *J. Catal.* **1982**, *74*, 55.
(2) (a) Davis, J. L.; Barteau, M. A. *Surf. Sci.* **1987**, *187*, 387. (b) Davis, J. L.; Barteau, M. A. *Surf. Sci.* **1988**, *197*, 123.
(3) McCabe, R. W.; Dimaggio, C. L.; Madix, R. J. *J. Phys. Chem.* **1985**, *89*, 854.
(4) (a) Anton, A. B.; Parmeter, J. E.; Weinberg, W. H. *J. Am. Chem. Soc.* **1985**, *107*, 5558. (b) Anton, A. B.; Parmeter, J. E.; Weinberg, W. H. *J. Am. Chem. Soc.* **1986**, *108*, 1823.
(5) Henderson, M. A.; Radloff, P. L.; White, J. M.; Mims, C. A. *J. Phys. Chem.* **1988**, *92*, 4111.
(6) Henderson, M. A.; Radloff, P. L.; Greenlief, C. M.; White, J. M.; Mims, C. C. *J. Phys. Chem.* **1988**, *92*, 4120.
(7) Henderson, M. A.; Radloff, P. L.; Greenlief, C. M.; White, J. M.; Mims, C. A. *J. Vac. Sci. Technol., A* **1988**, *6*, 769.
(8) (a) Tani, H.; Yasuda, H.; Araki, T. *J. Polym. Sci.* **1964**, *2B*, 933. (b) Tani, H.; Aoyagi, T.; Araki, T. *J. Polym. Sci.* **1964**, *2B*, 921. (c) Tani, H.; Oguni, N. *J. Polym. Sci.* **1965**, *3B*, 123. (d) Tani, H.; Araki, T.; Yasuda, H. *J. Polym. Sci.* **1966**, *4B*, 727. (e) Yasuda, H.; Tani, H. *Macromolecules* **1973**, *6*, 17.
(9) Ishida, S.-I. *J. Polym. Sci.* **1962**, *62*, 1.
(10) Jenkins, A. D.; Nyathi, J. Z.; Smith, J. D. *Eur. Polym. J.* **1982**, *18*, 149.
(11) Yamamoto, T.; Konagaya, S.; Yamamoto, A. *J. Polym. Sci., Polym. Lett. Ed.* **1978**, *16*, 7.
(12) Vogl, O. *J. Polym. Sci.* **1964**, *2A*, 4591.
(13) Natta, G.; Mazzanti, G.; Corradini, P.; Bassi, I. *Makromol. Chem.* **1960**, *37*, 156.
(14) Furukawa, J.; Saegusa, T.; Fujii, H.; Kawasaki, A.; Imai, H.; Fujii, Y. *Makromol. Chem.* **1960**, *37*, 149.
(15) (a) Furukawa, J.; Saegusa, T.; Tsuruta, H.; Fujii, H.; Tatano, T. *J. Polym. Sci.* **1959**, *36*, 546. (b) Furukawa, J.; Saegusa, T.; Tsuruta, T.; Fujii, H.; Kawasaki, A.; Tatano, T. *Makromol. Chem.* **1959**, *33*, 32.
(16) Hisatsume, I. C. *Spectrochim. Acta* **1983**, *39A*, 853.
(17) Madix, R. J.; Yamada, T.; Johnson, S. W. *Appl. Surf. Sci.* **1984**, *19*, 43.
(18) Mitchell, G. E.; Radloff, P. L.; Greenlief, C. M.; Henderson, M. A.; White, J. M. *Surf. Sci.* **1987**, *183*, 403.

0002-7863/89/1511-1185$01.50/0

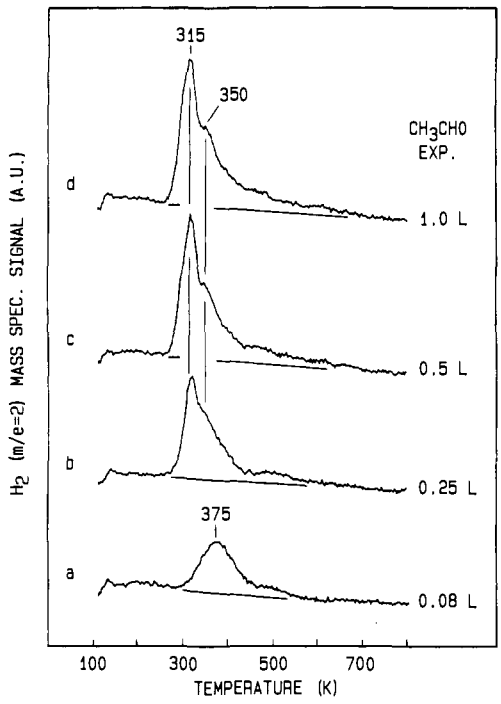

Figure 1. H_2 (m/e = 2) TPD spectra from various CH_3CHO exposures at 110 K on Ru(001).

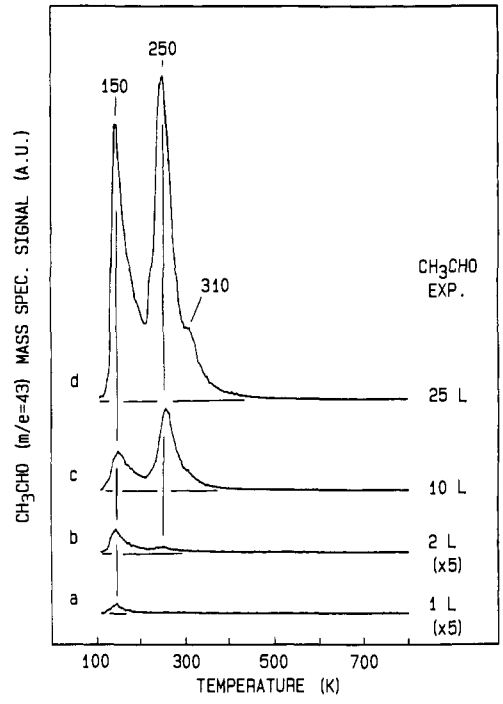

Figure 2. CH_3CHO (m/e = 43) TPD spectra from various CH_3CHO exposures at 110 K on Ru(001).

spectrometer is a 127° cylindrical sector type with stationary monochromator and analyzer defining a total scattering angle of 120°. All spectra were taken in the specular direction with a primary beam energy of 6.6 ± 0.3 eV and resolution of 10-meV full-width at half-maximum.

The mounting, cleaning, heating, and cooling of the Ru(001) is detailed elsewhere.[5] High-purity CH_3CHO (99.9% minimum purity), CH_3CDO (99+% C), and CD_3CDO (98+% D) were further purified by several freeze–pump–thaw cycles in liquid nitrogen. Exposures were made through a directional doser consisting of a 0.5-cm-i.d. stainless steel tube connected by a leak valve to the gas-handling system. Relative exposures were based on time in front of the doser at a constant acetaldehyde flux, which resulted in a 1×10^{-10} Torr pressure rise detected at the system's ion gauge. Actual exposures, correcting for the ion gauge sensitivity factor of CH_3CHO, were calibrated by back-filling experiments. The crystal was held at 110 K for all doses unless otherwise mentioned. Temperature-programmed ramp rates were 6.2 K/s.

3. Results

3.1. TPD. The H_2 TPD spectra of various CH_3CHO exposures on clean Ru(001) at 110 K are shown in Figure 1. Exposures of CH_3CHO below 0.08 langmuir (1 langmuir = 1×10^{-6} Torr·s) yield desorption-limited H_2 (375 K) with some high-temperature reaction-limited H_2 (>400 K). Larger exposures lead to a reaction-limited H_2 peak at 315 K with a shoulder at 350 K. The H_2 TPD peak area saturates between 0.5- and 1.0-langmuir CH_3CHO. The maximum H coverage is about 0.44 ML (1 ML equals 1 species per surface Ru atom). CO TPD (see Figure 7) consists of a single, desorption-limited peak at 460 K, which also saturates between 0.5- and 1.0-langmuir CH_3CHO with a maximum coverage of 0.11 ML. A trace amount of CO_2 (<0.01 ML) desorbs at 440 K (not shown).

No CH_3CHO desorbs below a 1-langmuir exposure, but for higher exposures a small TPD peak appears at 150 K due to multilayer desorption (Figure 2). A second TPD peak develops at 250 K from a 2-langmuir exposure and dominates as the exposure is increased from 2 to 25 langmuir. The 250 K peak is not saturated after a 25-langmuir exposure. A third CH_3CHO peak is resolved at 310 K for the 25-langmuir exposure.

Figure 3 shows the H_2, HD (m/e = 3), and D_2 (m/e = 4) TPD spectra from 10-langmuir CH_3CDO on Ru(001). The H_2 spectrum resembles those of Figure 1 except that less H_2 is desorbed above 350 K. The amount of D desorbed (as HD and D_2) above 350 K is comparatively greater than the amount of H desorbed (as H_2). The 357 K HD and 367 K D_2 peaks are proportionally larger in comparison to their respective 315 K peaks than the 350 K H_2 peak is. The same holds for the HD and D_2 peaks observed above 400 K.

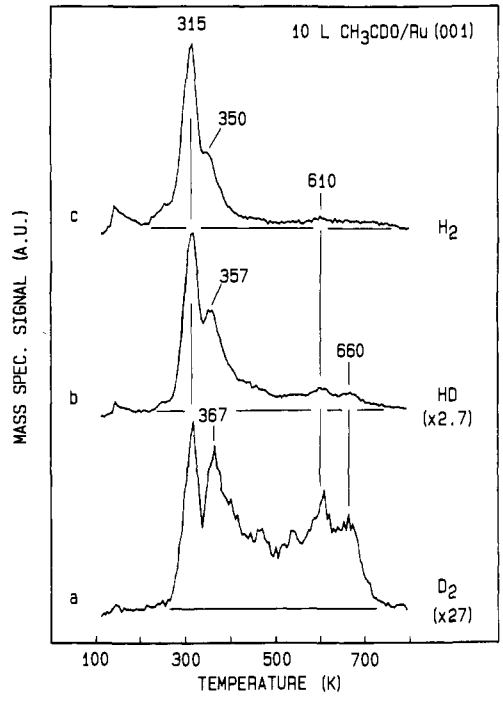

Figure 3. H_2 (m/e = 2), HD (m/e = 3), and D_2 (m/e = 4) TPD spectra from 10-langmuir CH_3CDO at 110 K on Ru(001).

3.2. +SSIMS. Figure 4 shows the +SSIMS spectra of various exposures of CH_3CHO on clean Ru(001) at 110 K. Ions between m/e = 96 and 104 are from Ru^+. CH_3^+ (m/e = 15) is the dominant ion for exposures below 0.5 langmuir, with weaker signals from $(CH_3CHO)H^+$ (m/e = 45) and CH_3CO^+ (m/e = 43). Very weak signals from K^+ (m/e = 39), Al^+ (m/e = 27), and Na^+ (m/e = 23) are due to trace impurities in the crystal.[5] There is no intensity from ions between m/e = 45 and 96 below an exposure of 0.5 langmuir. Between 0.5 and 1.0 langmuir the $(CH_3CHO)H^+$, CH_3CO^+, CHO^+ (m/e = 29), $C_2H_3^+$ (m/e = 27), and $C_2H_2^+$ (m/e = 26) signals increase significantly. Above 1.0 langmuir signals from $(CH_3CHO)_n$ species appear at m/e = 89

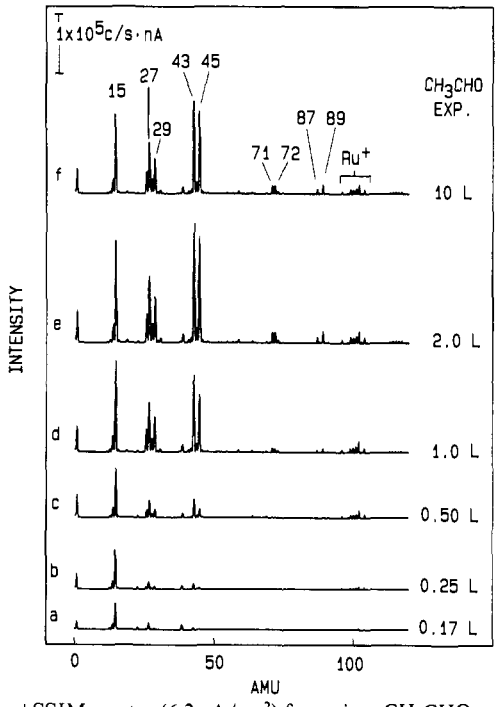

Figure 4. +SSIM spectra (6.2 nA/cm²) for various CH_3CHO exposures at 110 K on Ru(001).

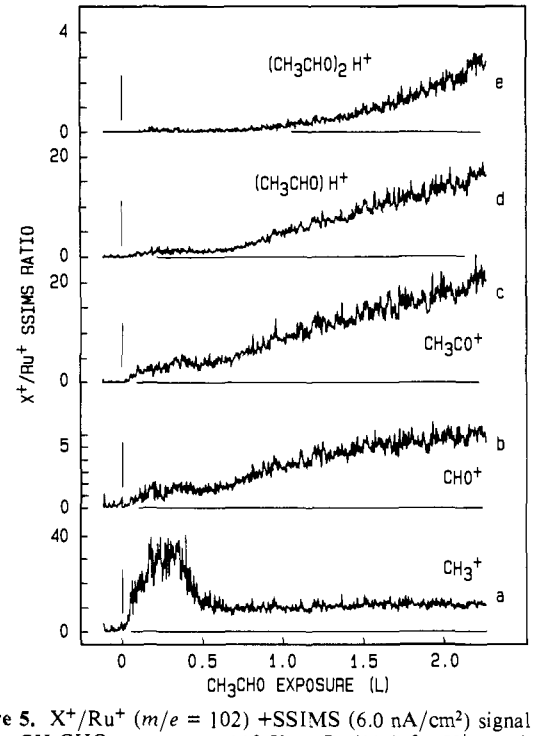

Figure 5. X^+/Ru^+ (m/e = 102) +SSIMS (6.0 nA/cm²) signal ratios versus CH_3CHO exposure at 110 K on Ru(001) for X^+ equal to (a) CH_3^+ (m/e = 15), (b) CHO^+ (m/e = 29), (c) CH_3CO^+ (m/e = 43), (d) $(CH_3CHO)H^+$ (m/e = 45), and (e) $(CH_3CHO)_2H^+$ (m/e = 89). Note ordinate scale differences for each spectrum.

$((CH_3CHO)_2H^+)$, 87 $((CH_3CHO)(CH_3CO)^+)$, 72 $((CH_3CHO)(CHCH_3)^+)$, and 71 $((CH_3CHO)(CCH_3)^+)$.

Figure 5 shows the +SSIM signal ratios of X^+/Ru^+ as a function of CH_3CHO exposure on Ru(001) at 110 K for X^+ equal to $(CH_3CHO)_2H^+$, $(CH_3CHO)H^+$, CH_3CO^+, and CH_3^+. Division by the Ru^+ signal (m/e = 102) was done to normalize the +SSIMS spectra. The CH_3^+/Ru^+ ratio rises as the exposure begins, maximizes at about 0.2 langmuir, and then attenuates above 0.4 langmuir and remains constant for exposures from 0.65 to 2 langmuirs. The 0.65-langmuir exposure roughly saturates the H_2 TPD (Figure 1). Attenuation of the CH_3^+/Ru^+ ratio at

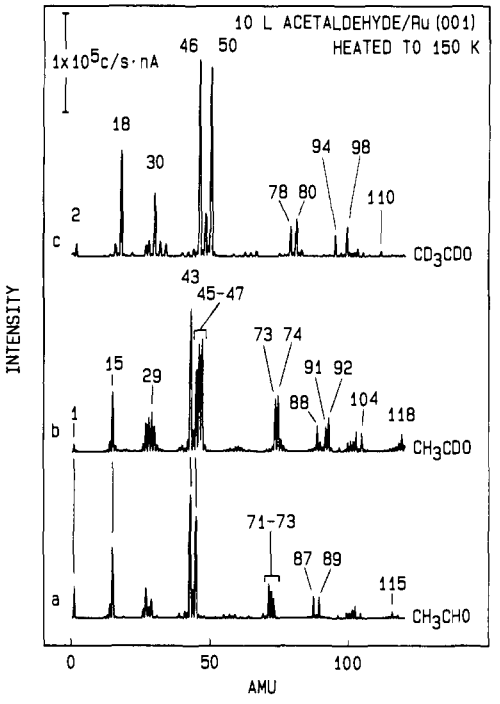

Figure 6. +SSIM spectra (7.0 nA/cm²) of 10-langmuir CH_3CHO (a), CH_3CDO (b), and CD_3CDO (c) at 110 K on Ru(001) after heating to 150 K.

0.4 langmuir does not result from decreased CH_3^+ intensity but from an increase in the Ru^+ intensity (Figure 4). The CHO^+/Ru^+, CH_3CO^+/Ru^+, and $(CH_3CHO)H^+/Ru^+$ ratios are small (<5) between 0 and 0.65 langmuir, and the $(CH_3CHO)_2H^+/Ru^+$ ratio is near zero. After the CH_3^+/Ru^+ ratio levels off at 0.65 langmuir the CHO^+/Ru^+, $(CH_3CHO)_2H^+/Ru^+$ ratio increases slightly between 0.65 and 1.5 langmuir but grows rapidly above 1.5 langmuir.

The +SSIMS ions greater than m/e = 45 in Figures 4 and 5 are not attributable to the multilayer CH_3CHO; +SSIMS ions from $(CH_3CHO)_n$ species [$(CH_3CHO)_2(CHCH_3)^+$ (m/e = 115), $(CH_3CHO)_2H^+$ (m/e = 89), $(CH_3CHO)(CH_3CO)^+$ (m/e = 87), $(CH_3CHO)(CHCH_3)^+$ (m/e = 72), and $(CH_3CHO)(CHCH_2)^+$ (m/e = 71)] are observed after desorption of the multilayer by heating to 150 K (Figure 6). These ions are also not from a +SSIMS event that forms multimers due to the close packing of the first layer since they are not observed at exposures that just saturate the first layer (Figure 4). Identification of each ion is facilitated by use of CH_3CDO and CD_3CDO (Figure 6). Assignments of these ions are shown in Table I.

The +TPSSIM (temperature-programmed) spectra of several pertinent ions from 10-langmuir CD_3CDO are shown in Figure 7 with the TPD spectra of D_2 (m/e = 4), CO (m/e = 28), and CD_3CDO (m/e = 48). Each CD_3CDO-related ion signal decreases, but does not go to zero, upon desorption of the multilayer and remains relatively constant between 150 and 250 K. They slowly rise upon desorption of the CD_3CDO peak at 250 K, and then maximize and abruptly decay coincident with the 305 K CD_3CDO and 315 K D_2 TPD peaks. Only the CD_3^+, CDO^+, CD_3CO^+, and $(CD_3CDO)D^+$ signals retain significant intensity above 350 K, and all four of them attenuate coincident with the 448 K D_2 peak. The Ru^+ (m/e = 102) signal rises slightly during desorption of the multilayer, remains constant to about 300 K, and then rises to about 450 K and attenuates as CO desorbs.

3.3. HREELS. The HREEL spectra of various CH_3CHO exposures on Ru(001) at 110 K are shown in Figure 8. The 0.17-langmuir spectrum is dominated by losses at 2970, 1395–1340, 1095, 915, and 605 cm^{-1} (Figure 8a). Losses at 1965 and 450 cm^{-1} result from background CO adsorbed during data collection. Absence of a loss between 1750 and 1450 cm^{-1} indicates that the C=O bond of CH_3CHO is rehybridized. In the region between 1450 and 1150 cm^{-1}, a similar analysis with 0.17-langmuir

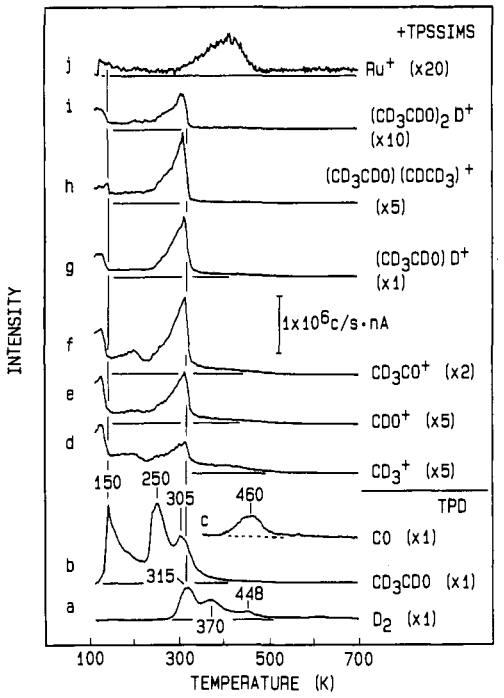

Figure 7. TPD for (a) D_2 (m/e = 4), (b) CD_3CDO (m/e = 48), and (c) CO (m/e = 28) and +TPSSIMS (6.5 nA/cm^2) for (d) CD_3^+ (m/e = 18), (e) CDO^+ (m/e = 30), (f) CD_3CO^+ (m/e = 46), (g) $(CD_3CDO)D^+$ (m/e = 50), (h) $(CD_3CDO)(CDCD_3)^+$ (m/e = 80), (i) $(CD_3CDO)_2D^+$ (m/e = 98), and (j) Ru^+ (m/e = 102) from 10-langmuir CD_3CDO at 110 K on Ru(001).

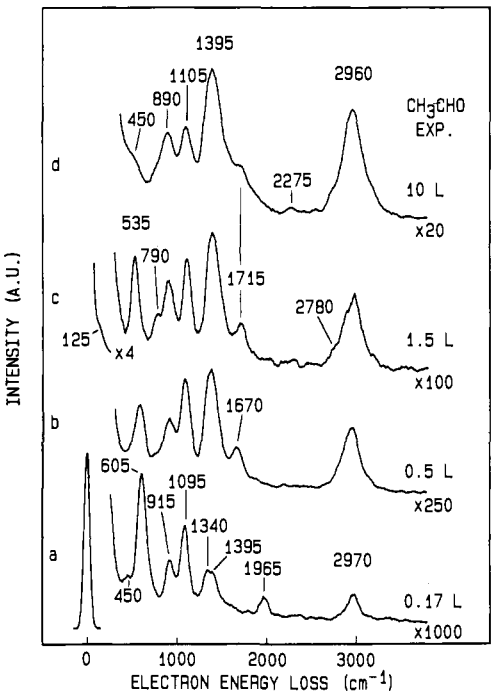

Figure 8. HREELS exposure set of CH_3CHO at 110 K on Ru(001).

CD_3CDO, shown in Figure 9, reveals only a weak loss at 1380 cm^{-1}. After 0.5-langmuir CH_3CHO, a 1670-cm^{-1} loss appears, accompanied by slight shifts and intensity changes in the other losses (Figure 8b). CO accumulation from background is inhibited by the coverage of the parent molecule. As the exposure is increased to 1.5 langmuirs, new losses appear at 2780, 1715, 790, and 125 cm^{-1} attributable to multilayer CH_3CHO.[3,16,19] A 10-langmuir exposure substantially attenuates the 535-cm^{-1} loss, and

(19) Hollenstein, H.; Günthard, Hs. H. *Spectrochim. Acta* **1971**, *27A*, 2027.

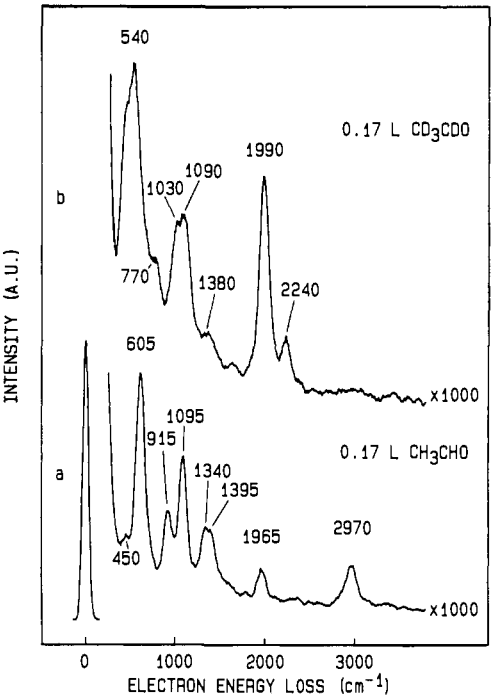

Figure 9. HREEL spectra of 0.17-langmuir CH_3CHO (a) and CD_3CDO (b) at 110 K on Ru(001).

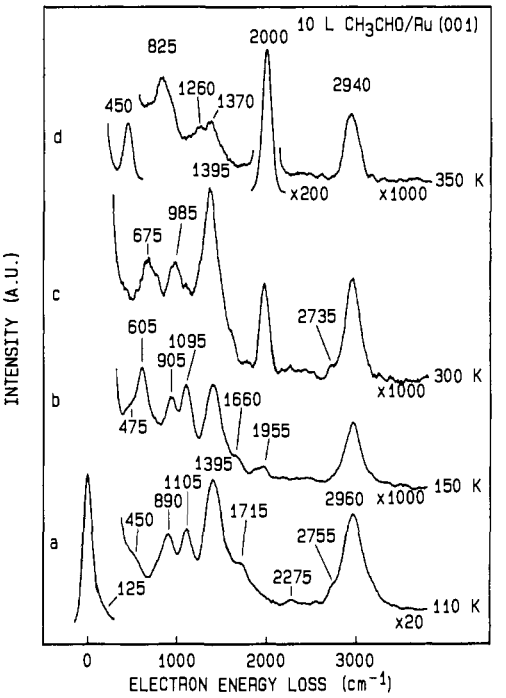

Figure 10. HREEL spectra of 10-langmuir CH_3CHO at 110 K (a) followed by heating to (b) 150 K, (c) 300 K, and (d) 350 K. Spectra obtained after cooling to 110 K.

a weak loss appears at 2275 cm^{-1}. The spectral line widths increase at large CH_3CHO exposures due to increased disorder of the adlayer.

The HREEL spectrum of 10-langmuir CH_3CHO at 110 K is repeated in Figure 10a. When this surface is heated to 150 K, desorbing some CH_3CHO, the 2755-, 2275-, 1715-, and 125-cm^{-1} losses disappear (Figure 10b). The remaining losses do not change significantly, but an intense loss at 605 cm^{-1} reappears, which was hidden in the exposure set (Figure 8) by multilayer CH_3CHO. Also, weak losses appear at 1955 and 475 cm^{-1} (residual atop CO) and at 1660 cm^{-1} (Figure 8b). The HREEL spectra of ≥5-langmuir CH_3CHO, CH_3CDO, and CD_3CDO after heating to 150 K (Figure 11) indicate that the majority of the loss intensity

Table I. Dominant +SSIMS Ions from 10-langmuir CH_3CHO, CH_3CDO, and CD_3CDO on Ru(001) at 110 K Heated to 150 K

amu	CH_3CHO	CH_3CDO	CD_3CDO
15	CH_3^+	CH_3^+	CD_3^+
18			
29	$H(CO)^+$	$H(CO)^+$	
30		$D(CO)^+$	$D(CO)^+$
43	CH_3CO^+	CH_3CO^+	
44	CH_3CHO^+		
45	$(CH_3CHO)H^+$	CH_3CDO^+	
46		$(CH_3CDO)H^+$	CD_3CO^+
47		$(CH_3CDO)D^+$	
48			CD_3CDO^+
50			$(CD_3CDO)D^+$
71	$(CH_3CHO)(CHCH_2)^+$		
72	$(CH_3CHO)(CHCH_3)^+$		
73	$(CH_3CHO)(CHCN_3)H^+$	$(CH_3CDO)(CDCH_2)^+$	
74		$(CH_3CDO)(CDCH_3)^+$	
75		$(CH_3CDO)(CDCH_3)H^+$	
76		$(CH_3CDO)(CDCH_3)D^+$	
78			$(CD_3CDO)(CDCD_2)^+$
80			$(CD_3CDO)(CDCD_3)^+$
82			$(CD_3CDO)(CDCD_3)D^+$
87	$(CH_3CHO)(CH_3CO)^+$		
88		$(CH_3CDO)(CH_3CO)^+$	
89	$(CH_3CHO)_2H^+$		
91		$(CH_3CDO)_2H^+$	
92		$(CH_3CDO)_2D^+$	
94			$(CD_3CDO)(CD_3CO)^+$
98			$(CD_3CDO)_2D^+$
103	*a*		
104		$(CH_3CDO)(CH_3CO)O^+$	
110			$(CD_3CDO)(CD_3CO)O^+$
115	$(CH_3CHO)_2(CHCH_3)^+$		
118		$(CH_3CDO)_2(CDCH_3)^+$	
127			*a*

[a] Undetected.

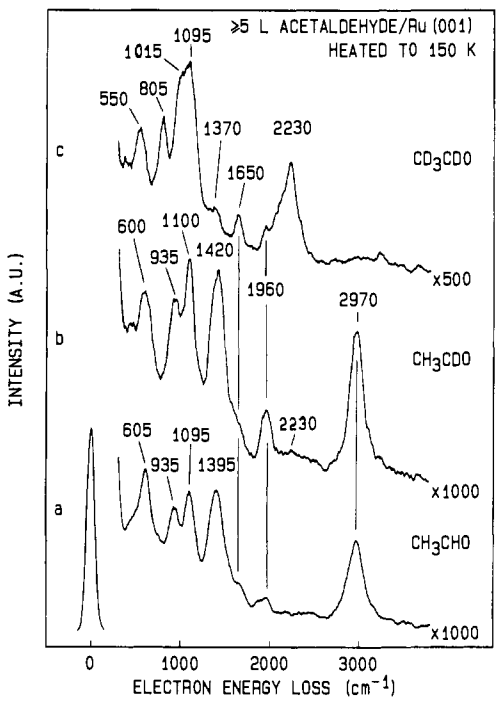

Figure 11. HREEL spectra of 10-langmuir CH_3CHO (a), 25-langmuir CH_3CDO (b), and 5-langmuir CD_3CDO (c) at 110 K on Ru(001) after desorption of the multilayer by heating to 150 K. Spectra obtained after cooling to 110 K.

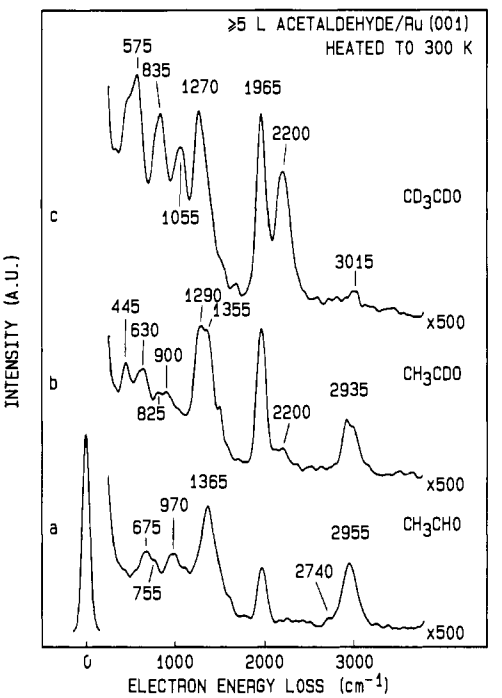

Figure 12. HREEL spectra of 10-langmuir CH_3CHO (a), 25-langmuir CH_3CDO (b), and 5-langmuir CD_3CDO (c) at 110 K on Ru(001) after heating to 300 K. Spectra obtained after cooling to 110 K.

between 1500 and 1300 cm^{-1} in the CH_3CHO (a) and CH_3CDO (b) spectra shifts below 1100 cm^{-1} for CD_3CDO (c). This suggests that the intensity at about 1400 cm^{-1} in the former two molecules results primarily from methyl deformation modes. The strong loss at 1095 cm^{-1} does not shift for these three molecules. Weak losses at 1645 and 1370 cm^{-1} are resolved in the CD_3CDO spectrum.

The 150 K HREEL spectrum of CH_3CHO does not change until the surface is heated above 250 K (Figure 10) with the exception that the 1670-cm^{-1} loss disappears after heating to 200 K (not shown). Figure 10c shows the 10-langmuir CH_3CHO HREEL spectrum after heating to 300 K, at which temperature the majority of the 250 K CH_3CHO TPD peak has desorbed (Figure 2) but little or no H_2 has desorbed (Figure 1). The 1095- and 605-cm^{-1} losses in Figure 10b are linked to the 250 K

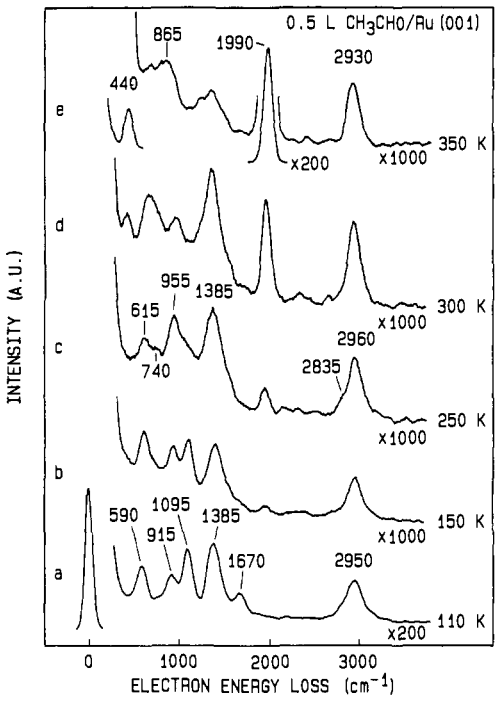

Figure 13. HREEL spectra of 0.5-langmuir CH_3CHO at 110 K (a) followed by heating to (b) 150 K, (c) 250 K, (d) 300 K, and (e) 350 K. Spectra obtained after cooling to 110 K.

CH_3CHO desorption state since they diminish after heating to 300 K, leaving losses at 2955, 2735, 1395, 985, and 675 cm^{-1} (Figure 10c). Comparison of the HREEL spectra of ≥5-langmuir CH_3CHO, CH_3CDO, and CD_3CDO heated to 300 K (Figure 12) indicates that the loss intensity in the 1500–1300-cm^{-1} region does not shift very much upon isotopic labeling, unlike spectra from identical exposures heated between 150 and 250 K (Figure 11). A weak loss at 3015 cm^{-1} in the CD_3CDO spectrum (Figure 12c) indicates some incorporation of background H has occurred upon heating to 300 K.

Heating 10-langmuir CH_3CHO to 350 K (Figure 10d) results in substantial decomposition of the adlayer as evidenced by intense losses from atop CO at 2000 and 450 cm^{-1} and by the 320 K H_2 desorption (Figure 1). Remaining losses appear at 2940, 1370–1260, and 825 cm^{-1}.

The HREELS annealing series of 0.5-langmuir CH_3CHO (Figure 13) is similar to the series for exposures greater than 5 langmuirs. TPD data indicate that the first layer is nearly saturated after a 0.2-langmuir exposure and that a multilayer has not formed. Absence of a 1715-cm^{-1} loss confirms the latter (Figure 13a). The 1670-cm^{-1} loss disappears after heating to 150 K (Figure 13b). The same loss from higher exposures disappears after heating to 200 K. HREEL spectra of 0.5-langmuir CH_3CHO heated above 150 K (Figure 13b–d) are remarkably similar to their respective 10-langmuir HREEL spectra (Figure 10) despite the fact that the latter exposure exhibits substantial CH_3CHO desorption at 250 K.

4. Discussion

We now turn to a discussion of the above results and the presentation of a model that provides a consistent interpretation and does not conflict with other work. While other interpretations, particularly of the two- and three-dimensional polymerization, are possible, our model gives a very satisfying picture. The discussion is divided into two sections, dealing with the surface species observed below and above 250 K. The significance of this temperature centers on the 250 K CH_3CHO desorption state, which we believe results from decomposition of CH_3CHO polymerized in three dimensions *above* the Ru(001) surface. The issue of acetaldehyde polymerization is addressed in the first section, and the chemistry that leads to the TPD products (H_2, CO, and trace CO_2) is discussed in the second section.

Table II. Assignment of the HREELS Loss Frequencies (cm^{-1}) for 0.17-langmuir Acetaldehyde on Ru(001) at 110 K to a Surface Polymer[a]

	0.17-langmuir CX_3CYO on Ru(001) at 110 K		
	X = Y = H	X = H, Y = D	X = Y = D
$\nu_a(CX_3)$			
$\nu_s(CX_3)$	2970	2980	2240
$\nu(CY)$	nr	nr	nr
$\delta_a(CX_3)$			
$\delta_s(CX_3)$	1395	1420	1030
$\nu_a(OCO)$	1340 (nr)	nr	1380
$\nu_s(OCO)$	1095	1100	1090
$\nu(CC)$			
$\rho(CX_3)$	915	940	770
$\delta(CY)$			
$\delta(OCO)$	605	580	540

[a] Key: nr, not resolved; s, symmetric; a, asymmetric; ν, stretch; δ, deformation; ρ, rock.

Chart I

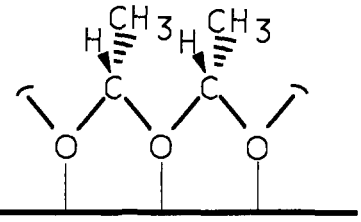

4.1. Surface Species below 250 K. We propose four different acetaldehyde species on Ru(001) below 250 K. These are CH_3CHO polymerized in two dimensions *across* the surface and $\eta^1(O)$ CH_3CHO, multilayer CH_3CHO, and CH_3CHO polymerized in three dimensions *above* the surface. These species appear as a function of CH_3CHO exposure in HREELS and +SSIMS in the order mentioned above. They are discussed below.

4.1.1. Polymerization across the Surface, 0–0.4 langmuir. Low CH_3CHO exposures (≤0.4 langmuir) on Ru(001) at 110 K are characterized by an intense CH_3^+ +SSIMS signal (Figures 4 and 5), CO, and H_2 in TPD, and HREELS losses at 2970, 1395–1340, 1095, 915, and 605 cm^{-1} (Figure 8a). Assignment of these losses is aided by the absence of intensity between 1700 and 1400 cm^{-1} where typical ν(C=O) frequencies are observed for $\eta^1(O)$-bound carbonyls.[4,20-22] Three explanations for the absence of this loss are (1) decomposition upon adsorption, (2) bonding in an $\eta^2(C,O)$ configuration, and (3) polymerization. HREELS losses from CO (1965 and 450 cm^{-1}), the major O-containing TPD product in Figure 8a, are weak, indicating little, if any, decomposition upon adsorption.

$\eta^2(C,O)$ CH_3CHO can also be excluded on the basis of the HREEL spectra of 0.17-langmuir CH_3CHO and CD_3CDO at 110 K (Figure 9). The majority of loss intensity between 1500 and 1300 cm^{-1} in the CH_3CHO spectrum is attributed to $\delta(CH_3)$ modes, since very little intensity is observed in this region for CD_3CDO. $\eta^2(C,O)$ acetaldehyde, which we have previously characterized from hydrogenation of ketene (CH_2CO and CD_2CO) on Ru(001),[5] has a stront ν(CO) loss at 1270 cm^{-1} that does not shift for CD_3CDO. Absence of a strong feature in the HREEL spectrum of 0.17-langmuir CD_3CDO (Figure 9b) indicates that low acetaldehyde exposures on Ru(001) do not form $\eta^2(C,O)$ CH_3CHO.

The remaining possibility, and the one we favor, is that acetaldehyde polymerizes in two dimensions upon adsorption, changing the C=O bond to a C—O bond and shifting the ν(CO) loss below

(20) (a) Avery, N. R. *Surf. Sci.* **1983**, *125*, 771. (b) Avery, N. R. *Langmuir* **1985**, *1*, 162. (c) Avery, N. R. *J. Vac. Sci. Technol., A* **1985**, *3*, 1459.

(21) Avery, N. R.; Anton, A. B.; Toby, B. H.; Weinberg, W. H. *J. Electron Spectrosc. Relat. Phenom.* **1983**, *29*, 233.

(22) Avery, N. R.; Weinberg, W. H.; Anton, A. B.; Toby, B. H. *Phys. Rev. Lett.* **1983**, *51*, 682.

Table III. HREELS Frequencies (cm^{-1}) of Polymerized Acetaldehyde on Ru(001) between 150 and 250 K for Exposures ≥5 langmuir[a] and IR Frequencies of Crystalline Polyacetaldehyde[b]

	CX_3CYO[a]			
	X = H, Y = H	X = H, Y = D	X = D, Y = D	crystalline $(CH_3CHO)_n$[b]
$\nu_a(CX_3)$	2970	2970	2230	2980†*
$\nu_s(CX_3)$				2930*
$\nu(CY)$	nr	2230	nr	2905*
$\delta_a(CX_3)$				1443, 1400
$\delta_s(CX_3)$	1395	1420	1015	1385†, 1347
$\nu_a(OCO)$	nr	nr	1370	1187, 1158, 1122†
$\nu_s(OCO)$	1095	1100	1095	1083†, 1040
$\nu(CC)$				na[c]
$\rho(CX_3)$	935	935	805	973†, 933†
$\delta(CY)$				850, 835*
δ(OCO)	*605*	*600*	*550*	*na*

[a] This work. [b] Reference 14. Asterisks indicate our assignment of their unassigned data. Daggers indicate most intense IR bands. [c] Key: na, not assigned.

1200 cm^{-1}. We assign the intense HREELS loss at 1095 cm^{-1} to the ν_s(OCO) mode of polymerized acetaldehyde (Chart I), with the remaining losses assigned in Table II. There is a strong similarity between these loss frequencies and the IR bands of polymerized CH_3CHO (see Table III).[14] Previous examples of formaldehyde (H_2CO) polymerization across metal surfaces in UHV also support this conclusion (see ref 23 and references therein). H_2CO, however, is much more reactive on transition metals, exhibiting substantial decomposition upon adsorption above 100 K. The formation of the proposed CH_3CHO two-dimensional surface polymer at 110 K is linked to the inability of the CH_3CHO carbonyl carbon to bind to the surface and the instability of the η^1(O) configuration at low coverages. The former is probably due to steric interactions of the methyl group with the surface. We propose that when the surface becomes nearly covered with this two-dimensional polymer, η^1(O) CH_3CHO can begin to accumulate. The η^2(C,O) species probably does form on Ru(001) at higher adsorption temperatures, since it is observed after decomposition of the surface polymer at 250 K (to be discussed) and since Avery et al.[21,22] have observed η^2(C,O) acetone on Ru(001) as low as 190 K. The instability of the η^1(O) species at 110 K is evidenced by the absence of a ν(CO) loss in HREELS between 1700 and 1400 cm^{-1} for low CH_3CHO exposures (Figures 8a and 9).

Although HREELS data support the assignment of a surface polymer, there is no evidence in +SSIMS for ions associated with $(CH_3CHO)_n$ at low acetaldehyde exposures. Instead, the dominant ion is CH_3^+. Apparently, when the polymer is coordinated across the surface, the yield of positive ions associated with the skeleton of the polymer, which is bound to the surface, is low and the yield of CH_3^+, which is away from the surface, is high. This +SSIMS behavior is consistent with results from ethylidyne (CCH_3) on Ru(001), which shows very strong CH_3^+ signals but weak $C_2H_x^+$ signals.[24,25] When the polymer grows above the surface the yield of $(CH_3CHO)_n$ ions increases significantly (to be discussed).

We propose that CH_3CHO polymerization across the surface results from reaction of neighboring CH_3CHO molecules transiently bound at η^1(O). This mechanism is supported by HREELS and TPD results of 0.5-langmuir CH_3CHO (Figures 2 and 13), which show that η^1(O) CH_3CHO does not desorb after heating to 150 K but incorporates into the polymer (see below).

Decomposition of the surface polymer, as indicated by the loss of ν_s(OCO) intensity, occurs at about 250 K, according to the HREELS annealing set of 0.5-langmuir CH_3CHO (Figure 13), but does not result in either CH_3CHO desorption or CH_3CHO decomposition. This is evidenced by the absence of CH_3CHO

(23) Henderson, M. A.; Mitchell, G. E.; White, J. M. *Surf. Sci.* **1987**, *188*, 206.
(24) Henderson, M. A.; Mitchell, G. E.; White, J. M. *Surf. Sci.*, in press.
(25) Greenlief, C. M.; Radloff, P. L.; Zhou, X.-L.; White, J. M. *Surf. Sci.* **1987**, *191*, 93.

Chart II

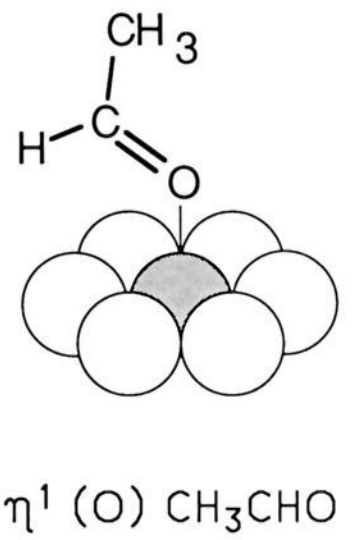

η^1 (O) CH_3CHO

in TPD at exposures below 1 langmuir and the absence of atop CO in HREELS at 250 K (Figure 13c). Instead, the surface polymer converts into η^2(C,O) CH_3CHO (to be discussed).

4.1.2. η^1(O) CH_3CHO, 0.4–0.6 langmuir. η^1(O) acetaldehyde is evidenced on Ru(001) at CH_3CHO exposures between 0.4–0.6 langmuir and at temperatures below 200 K by a ν(CO) HREELS loss at 1670 cm^{-1} (Figures 8b and 11). This loss is about 50-cm^{-1} red-shifted from the solid-phase value.[3,16,19] McCabe et al. have previously observed η^1(O) CH_3CHO on Pt(S)[6(111)×(100)].[3] Additionally, Avery has observed η^1(O) acetone ($(CH_3)_2CO$) on Pt(111),[20] and Anton et al. have observed η^1(O) H_2CO on Ru(001).[4] The bonding of these species to metal surfaces involves lone-pair donation from the O to the metal as indicated in Chart II). η^1(O) acetaldehyde is observed on Ru(001) when the first layer is near saturation, between 0.4 and 0.6 langmuir. It becomes obscured when the multilayer forms. The two-dimensional polymer is the preferred bonding structure when the surface is not crowded. At higher surface coverages, η^1(O) CH_3CHO apparently occupies isolated sites not used by the surface polymer.

The decrease in the CH_3^+/Ru^+ +SSIMS ratio between exposures of 0.4 and 0.6 langmuir at 110 K (Figure 5) coincides roughly with the exposure range at which η^1(O) CH_3CHO is observed in HREELS. The CH_3^+/Ru^+ ratio decreases primarily because the Ru^+ yield increases with η^1(O) CH_3CHO formation and not because the CH_3^+ yield decreases (Figure 4). The other X^+/Ru^+ ratios are not affected in the same manner (Figure 5).

The HREELS annealing set of 0.5-langmuir CH_3CHO (Figure 13) indicates that η^1(O) CH_3CHO is unstable on Ru(001) above 150 K. Since no CH_3CHO desorption takes place at this exposure (Figure 2) and no CH_3CHO decomposition occurs below 300 K (Figure 13), disappearance of the 1670-cm^{-1} loss (ν(CO)) after heating to 150 K indicates that the ν^1(O) molecules incorporate into the surface polymer.

4.1.3. Multilayer CH_3CHO, >1 langmuir. For CH_3CHO exposures above about 1 langmuir, desorption of multilayer CH_3CHO occurs at 150 K (Figure 2), in agreement with previous studies.[3,26] The multilayer state is evidenced in HREELS by losses at 2780, 2275, 1715, 790, and 126 cm^{-1} (Figures 8c and 10a) assigned to ν(CH), [$\delta(CH_3)$ + $\rho(CH_3)$], ν(CO), δ(CH), and solid acetaldehyde lattice vibration, respectively.[3,16,19] The $\nu_s(CH_3)$, $\delta_s(CH_3)$, and $\rho(CH_3)$ losses cannot be differentiated from those of the polymer (to be discussed). The formation of the multilayer in HREELS coincides roughly with the CH_3CHO exposure that saturates the H_2 (and CO) TPD (Figure 1). Also, the +SSIMS *ion yield ratios for* CHO^+/Ru^+, CH_3CO^+/Ru^+, *and* $(CH_3CHO)H^+/Ru^+$ all increase for CH_3CHO exposures above 0.6 langmuir and are attributable to growth of the multilayer state (Figure 5).

4.1.4. Polymerization above the Surface, >1.5 langmuir. Although exposures of CH_3CHO above 1.0 langmuir result in multilayer formation, a new species also develops that we attribute to three-dimensional polymerization *above* the surface. The large desorption state at 250 K develops only after the H_2 TPD saturates

(26) Shanahan, K. L.; Muetteries, E. L. *J. Phys. Chem.* **1984**, *88*, 1996.

and after the multilayer appears and is attributable to decomposition of this polymerized CH_3CHO. Assuming a relatively constant sticking coefficient at 110 K, the amount of CH_3CHO still adsorbed after heating 25 langmuir above 150 K is far greater than what can be accommodated in the first surface layer. Polymerization above the surface is a suitable explanation for both the stability and quantity remaining. It is also significant that +SSIMS ions involving multimers of CH_3CHO are observed only for exposures >1.0 langmuir (Figures 4 and 5). These ions are not due to simple multilayer CH_3CHO since annealing above 150 K does not remove them from +SSIMS (Figures 6 and 7).

Additional evidence for polymerization above the surface at high CH_3CHO exposures is given by HREELS. Table III compares the HREEL losses of ≥5-langmuir CH_3CHO, CH_3CDO, and CD_3CDO heated to 150 K with the IR peaks of crystalline polyacetaldehyde catalyzed with a metal alkoxide.[14] There is good agreement between our HREELS data and the IR data for the crystalline polymer.

CH_3CHO polymerization in hydrocarbon solutions[8-14] requires low temperatures (<240 K) and the presence of an initiator, such as an inorganic acid or organometallic complex, to rehybridize the first CH_3CHO molecule and commence polymer growth. Crystalline and amorphous $(CH_3CHO)_n$ consists of chain structures, where the carbonyl oxygen of one molecule is bound to the carbonyl carbon of another molecule.[8,12] Ring formation has also been observed.[11] Our results suggest that CH_3CHO polymerization is initiated by the Ru(001) surface. The logical points for this initiation are the ends of the two-dimensional polymer chains, which form across the surface at lower exposures. Gaps in the three-dimensional polymer, which expose the first layer after desorption of the multilayer, are responsible for detection of small amounts of atop CO and η^1(O) CH_3CHO after annealing 10-langmuir CH_3CHO to 150 K (Figure 11).

Our results suggest that CH_3CHO polymerization above the surface does not occur unless a multilayer state is first formed. Large exposures of CH_3CHO on Ru(001) held above 150 K do not yield the 250 K CH_3CHO TPD peak. This suggest that the multilayer is required in UHV in order to provide a high enough concentration and sufficiently long residence time for physisorbed CH_3CHO to polymerize with the first layer. The ceiling temperature for polymer formation in solution is about 80 K higher (230 K).[8]

All three isotopically labeled acetaldehyde molecules (CH_3CHO, CH_3CDO, and CD_3CDO) have polymer decomposition peaks in TPD at about 250 and 310 K. The relative amount of acetaldehyde in the 250 K TPD peak versus the 310 K peak is much greater for 10-langmuir CH_3CHO (Figure 2) than for either CH_3CDO (not shown) or CD_3CDO (Figure 7). The 310 K peak for CH_3CHO is a small shoulder on the 250 K peak regardless of exposure. The 310 K peak for 10-langmuir CD_3CDO is much more intense (Figure 7). The difference between the 250 and 310 K CD_3CDO peaks is unclear since HREELS above 250 K is complicated by the losses of η^2(C,O) CD_3CDO.

It is interesting to note that decomposition of the polymer above the surface produces only monomeric CH_3CHO. Madix et al.[17] observed that decomposition of polymerized CH_3CHO on p(2×2) S-covered Ni(100) produced the ring species $[CH_3CHO]_3$ known as paraldehyde, as well as monomers.

4.2. Surface Species above 250 K. As mentioned previously, η^1(O) CH_3CHO is not stable on Ru(001) above about 150 K, and both polymer species (across and above the surface) decompose at 250 K. This section focuses on the species left on the surface after decomposition of the polymers.

4.2.1. η^2(C,O) CH_3CHO. We propose that η^2(C,O) CH_3CHO (Chart III) is the major species left on the surface following decomposition of the polymers at 250 K. HREELS losses after heating to 300 K (Figure 12) are compared in Table IV to the losses of η^2(C,O) CH_3CHO previously characterized from ketene hydrogenation on Ru(001).[5] There is good agreement. Absence of intense HREELS losses from atop CO in the HREEL annealing set of 0.5-langmuir CH_3CHO (Figure 13) and absence of TPD products other than CH_3CHO below 300 K (Figure 2) suggest

Table IV.[a] HREELS Frequencies (cm^{-1}) for η^2(C,O) Acetaldehyde from Dosed Acetaldehyde[b] and from Hydrogenated Ketene[c]

	acetaldehyde[b] (300 K)			ketene + H/D[c] (250 K)	
	CH_3CHO	CH_3CDO	CD_3CDO	CH_3CHO	CD_3CDO
$\nu_a(CX_3)$				3025 (os)	2230 (os)
$\nu_s(CX_3)$	2955	2935	2200	2930	2200
ν(CY)	2740	2200	nr	2755	nr
$\delta_a(CX_3)$					
$\delta_s(CX_3)$	1365	1355	1055	1365	1050
ν(CO)	nr	1290	1270	1275	1260
ν(CC)	1105 (nr)	nr	nr	1135	1095
$\rho(CX_3)$	970	900	835	975	850
δ(CY)	755	nr	nr	795 (os)	nr
δ(CCO)	675	630	575	655	620
π(CCO)				575 (os)	nr

[a] Key: δ, in-plane bend; π, out-of-plane bend; os, off-specular. [b] This work. [c] Reference 5.

Chart III

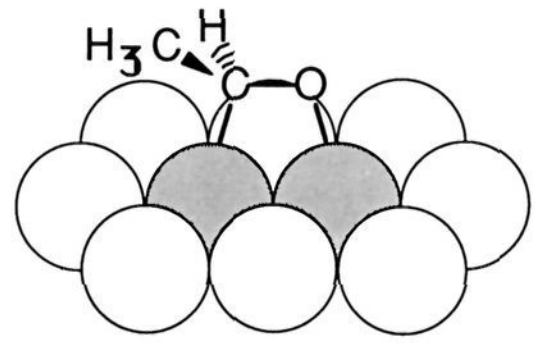

η^2 (C,O) CH_3CHO

that the η^2(C,O) species is the exclusive product of the surface polymer decomposition.

η^2(C,O) CH_3CHO is stable on Ru(001) to about 315 K, where H_2 appears in TPD and atop CO grows in HREELS. Its decomposition is very similar to that produced from ketene hydrogenation.[6] Both systems evolve H_2 almost exclusively in a sharp TPD peak at 315–330 K and result in strong CO losses in HREELS (Figures 10d and 13d). The decomposition of this species is summarized by

$$\eta^2(C,O)\ CH_3CHO \rightarrow C + 2H_2 + CO \qquad (1)$$

since CO is the major O-containing TPD product and since the majority of the H_2 desorbs at 315 K.

The H_2, HD, and D_2 TPD spectra from CH_3CDO (Figure 3) suggest a possible mechanism for decomposition of the η^2(C,O) species. A proportionally greater amount of D desorbs (as HD and D_2) above 330 K than does H (as H_2 and HD), suggesting that cleavage of the aldehydic C–H/C–D bond is not the first step in η^2(C,O) decomposition. Supporting this suggestion, little or no η^2(C,O) acetyl (CH_3CO), a very likely product of aldehydic C–H/C–D bond cleavage, is formed from η^2(C,O) CH_3CHO decomposition. η^2(C,O) CH_3CO is characterized by a strong ν(CO) HREELS loss at 1420 cm^{-1} and H_2 and CO_2 TPD states at 440 K, approximately 110 K higher than η^2(C,O) CH_3CHO.[5,6] The trace amount of CO_2 at 440 K from acetaldehyde may indicate that a trace of η^2(C,O) CH_3CO is formed from η^2(C,O) CH_3CHO decomposition. C–O bond cleavage is excluded since desorption-limited CO is the major O-containing TPD product. These observations favor CH_2–H or C–CH_3 cleavage as the initial step in η^2(C,O) CH_3CHO decomposition.

An isotope effect in the C–H bond cleavage could account for the proportionally greater amount of D_2 desorption above 350 K for CD_3CDO decomposition (Figure 7) than H_2 from CH_3CHO decomposition (Figure 1). There is also a proportionally greater amount of η^2(C,O) acetyl (the 448 K H_2, HD, and D_2 TPD peaks) formed from η^2(C,O) CD_3CDO decomposition (Figure 7) than from either CH_3CDO (Figure 3) or CH_3CHO (Figure 1). This does not imply that an aldehydic C–D bond is weaker than an

aldehydic C-H bond since very little η^2(C,O) CH_3CO is formed from η^2(C,O) CH_3CDO decomposition but probably that the aliphatic C-H bonds and/or the C-CH_3 bond are weaker than the aliphatic C-D bonds and/or the C-CD_3 bond. This, coupled with the shift in the 350 K peak temperature to 357 K for HD and 367 K for D_2 from CH_3CDO decomposition (Figure 2), indicates a small, but detectable, isotope effect in the decomposition of η^2(C,O) acetaldehyde.

4.2.2. Other Species. As mentioned above, very small amounts of η^2(C,O) CH_3CO are likely in the decomposition of η^2(C,O) CH_3CHO. This species is characterized by coincident desorption of H_2 and CO_2 at 450 K in TPD, CH_3^+, and CH_3CO^+ +SSIMS signals and an intense ν(CO) loss at 1420 cm^{-1}.[5,6] The ν(CO) mode of η^2(C,O) acetyl, produced from η^2(C,O) CH_3CHO decomposition in this study, is not clearly resolved by HREELS because its coverage is low. The CD_3^+ and CD_3CO^+ ions of Figure 7 attenuate coincident with the 448 K D_2 TPD state, indicating that some η^2(C,O) CD_3CO does result from CD_3CDO decomposition.

There is no evidence that η^2(C,O) CH_3CHO decomposition results in CCH_3 formation. The HREELS of CCH_3 should give a loss at 1100 cm^{-1} from the ν(CC) mode[24] but is not observed in Figure 13e from η^2(C,O) CH_3CHO decomposition. CCH_3 formation from CH_3CHO decomposition was observed by McCabe et al. on Pt(S)[6(111)×(100)].[3]

The decomposition of C_xH fragments is responsible for most of the H_2 desorption above 400 K. These fragments result from decomposition of η^2(C,O) CH_3CHO. However, since the amount of H_2 above 400 K is much less than that below 400 K, C_xH is a minority species in CH_3CHO decomposition. An HREELS loss at about 850 cm^{-1} in Figures 10d and 13e is due to the δ(CH) mode of C_xH, and losses in the 1400-1200-cm^{-1} region may be attributed in part to the ν(CC) mode.

5. Summary

A. Surface CH_3CHO Polymerization. HREELS results indicate that low CH_3CHO exposures (<0.4 langmuir) on Ru(001) at 110 K polymerize in two dimensions across the surface. The surface polymer is formed from the reaction of neighboring transiently adsorbed η^1(O) CH_3CHO molecules and decomposes exclusively to η^2(C,O) CH_3CHO at 250 K.

B. η^1(O) CH_3CHO. η^1(O) CH_3CHO is unstable with respect to two-dimensional polymer formation, and it is only observed at exposures near saturation of the first layer and at temperatures below 150 K. Above 150 K the η^1(O) species incorporates into the surface polymer.

C. Multilayer CH_3CHO. Multilayer CH_3CHO appears on Ru(001) for CH_3CHO exposures above 1 langmuir and desorbs in TPD at 150 K.

D. CH_3CHO Polymerization above the Surface. Two additional CH_3CHO TPD states (250 and 310 K) appear in TPD only for CH_3CHO exposures above 1.5 langmuir and do not saturate for a 25-langmuir exposure. These TPD states are associated with +SSIMS ions from dimers and trimers and are attributed to CH_3CHO polymerization in three dimensions above the surface. This polymerization requires a multilayer.

E. η^2(C,O) CH_3CHO. The HREEL spectra after heating CH_3CHO to 300 K resembles that of η^2(C,O) CH_3CHO obtained from ketene hydrogenation on Ru(001).[5] Decomposition of this species accounts for all the CO, H_2, and trace CO_2 observed in TPD. The maximum CH_3CHO decomposition coverage (0.11 ML) is reached after an exposure of about 0.5 langmuir.

Acknowledgment. Support of this work by National Science Foundation Grant CHE8505413 is gratefully acknowledged.

Registry No. CH_3CHO, 75-07-0; Ru, 7440-18-8.

Dimethyl Disulfide: Anion–Molecule Reactions in the Gas Phase at 300 K

Joseph J. Grabowski* and Lijian Zhang

Contribution from the Department of Chemistry, Harvard University, 12 Oxford Street, Cambridge, Massachusetts 02138. *Received July 22, 1988*

Abstract: The thermally equilibrated gas-phase anion–molecule reactions of dimethyl disulfide were examined in a helium bath gas at 0.3 Torr at 300 K by the flowing afterglow technique. All anions more basic than methanethiolate were observed to undergo reaction, but anions less basic than HS^- reacted too slowly to form observable products. Sulfur-centered nucleophiles slightly less basic than methanethiolate were found to undergo thiolate/disulfide interchange. Two bimolecular reaction pathways are proposed to account for the primary reaction products: substitution at sulfur and elimination across the carbon–sulfur bond. The elimination pathway involves initial formation of an ion–dipole complex containing thioformaldehyde and methanethiolate, which subsequently undergoes either addition to give a rearranged thiolate product or dissociation. The primary factor in determining whether an anion gives sulfur substitution or elimination products is the structure of the anion and not the nucleophile base strength. Anions at least as basic as methoxide and in which the charge is localized preferred to react by elimination across the carbon–sulfur bond, while all delocalized carbanion bases strongly preferred substitution at sulfur.

The importance of sulfur, demonstrated by the existence of a vast literature, is due to the variety of valence states for sulfur and sulfur's widespread occurrence in chemistry, in biology, in industry, in agriculture, and in air pollution among others. Limiting a discussion to reduced sulfur compounds would still encompass a variety of classes of molecules and span a number of disciplines from thiol/disulfide interchange reactions of biochemical systems to contributions to acid rain via the atmospheric sulfur cycle to desulfurization of fuel stocks. Narrowing the topic even further, much is now known about the reactivity of disulfides in the condensed phase, with the studies concentrating upon cleavage of the sulfur–sulfur bond. However, much less is understood about the nature of competition between reaction at sulfenyl sites versus carbon sites.

It appeared to us that a gas-phase ion–molecule investigation into the intrinsic chemistry displayed by unsolvated, uncomplexed anions reacting with unsolvated, unaggregated reduced sulfur systems would make an important contribution to efforts to thoroughly understand the chemistry of sulfur in all its applications.[1] By utilizing the techniques and approaches developed for

0002-7863/89/1511-1193$01.50/0